Volume 14, Issue 3, Page 145-150, 2025 https://doi.org/10.46810/tdfd.1691969 Research Article

BİNGÖL UNIVERSITY

Türk Doğa ve Fen Dergisi
Turkish Journal of Nature and Science
www.dergipark.gov.tr/tdfd

Strength Performance of 304 Series Steels Welded by Plasma Arc Method

Tanju TEKER[1*], Sinan AYDIN[2]

[1] Sivas Cumhuriyet University, Technology Faculty, Manufacturing Engineering Department, Sivas, Türkiye
[2] Sivas Cumhuriyet University, Technology Faculty, Mechatronics Engineering Department, Sivas, Türkiye
Tanju TEKER ORCID No: 0000-0001-7293-0723
Sinan AYDIN ORCID No: 0000-0003-2285-0906

**Corresponding author: tanjuteker@cumhuriyet.edu.tr*

(Received: 05.05.2025, Accepted: 12.08.2025, Online Publication: 26.09.2025)

Keywords
Plasma arc welding, AISI 304, Microstructure, Strength test

Abstract: Austenitic stainless steel has superior mechanical and corrosion performance and is used in many sectors. Welding is a commonly used method in the production of stainless-steel structures. Plasma transfer arc welding is a technique performed by an electric arc between tungsten electrodes. In this research, AISI 304 plates were welded using plasma welding. The joint interface was analyzed through scanning electron microscopy, optical microscopy, energy dispersive spectroscopy, X-Ray diffraction. The strength performance of the samples were assessed via tensile testing. The fracture surfaces of samples were studied by SEM. The PTA method achieved complete penetration in AISI 304 plate joint. The recorded seam widths were 6 mm for S1, 6.5 mm for S2, and 7 mm for S3. The samples exhibited strengths of 336 MPa at 70 A, 360 MPa at 80 A, and 374 MPa at 90A. All joints showed good strength.

Plazma Ark Yöntemiyle Kaynaklanan 304 Serisi Çeliklerin Dayanım Performansı

Anahtar Kelimeler
Plazma ark kaynağı, AISI 304, Mikroyapı, Mukavemet testi

Öz: Östenitik paslanmaz çelik, üstün mekanik ve korozyon performansına sahiptir ve birçok sektörde kullanılır. Kaynak, paslanmaz çelik yapıların üretiminde yaygın olarak kullanılan bir yöntemdir. Plazma transfer ark kaynağı, tungsten elektrotlar arasındaki elektrik arkı ile yapılan bir tekniktir. Bu araştırmada, AISI 304 plakalar plazma kaynağı kullanılarak kaynaklanmıştır. Birleşme arayüzeyi, taramalı elektron mikroskobu, optik mikroskop, enerji dağılımlı spektroskopi ve X-Ray diffraction ile analiz edilmiştir. Numunelerin mukavemet özellikleri, çekme testi ile değerlendirilmiştir. Numunelerin kırılma yüzeyleri SEM ile incelenmiştir. PTA yöntemi, AISI 304 plaka birleşme arayüzeyinde tam penetrasyon sağlamıştır. Kaydedilen dikiş genişlikleri S1 için 6 mm, S2 için 6,5 mm ve S3 için 7 mm'dir. Numuneler düşük ısı girdisi altında 336 MPa, orta ısı girdisi altında 360 MPa ve yüksek ısı girdisi altında 374 MPa mukavemet sergilemiştir. Tüm birleşimler iyi dayanım göstermiştir.

1. INTRODUCTION

Stainless steels are key materials in engineering. Austenitic stainless steels (ASS) are recognized for their excellent resistance to corrosion, high flexibility, and strong weldability [1]. In these steels, austenite is the primary phase at room temperature. AISI 304 is a stainless-steel grade commonly utilized in aerospace, chemical machinery, nuclear applications, and pressure vessels. ASS is more commonly chosen than other stainless-steel types because of its ease of welding [2,3]. Welding is indispensable in many fields such as chemical, oil and gas industries. Because various combinations of materials can be combined. However, the welding process can notably influence the mechanical properties of welded joints by altering the microstructure, leading to issues such as micro segregation, phase precipitation, pores, and cracks [4,5]. Plasma transferred arc welding (PTAW) has high efficiency and cleanliness quality. PTAW is the most reliable welding method for stainless steel with its ability to weld complex shapes. It is also recognized for being cost-effective and widely adopted [6,7]. PTAW has gained significant popularity in the manufacturing industry for metal joining in recent years. It is preferred over other arc methods due to its high speed, quality weld production and stable performance. Recently, numerous advancements have been made to enhance the stability of the PTAW process, as well as to improve penetration depth and weld quality [8-10]. Bodkhe et al. [11] reported the optimization of TIG welding of 304L materials.

Penetration depth was influenced by current, torch speed, and arc gap. In single pass conventional TIG, penetration is limited to 3 mm. Ramakrishnan et al. [12] investigated the strength performances and microstructure of TIG welded AISI 304 and AISI 316. The highest tensile strength was attained through welding with the peak current. AISI 308L welding wire provided the best results and enhanced mechanical properties.

This study aims to achieve the joining of AISI 304 plates in a single pass using plasma welding, without employing filler wire or a weld groove. Analyses of macrostructure, microstructure, phase composition, mechanical properties, and fracture surfaces of welded samples were conducted.

2. MATERIAL AND METHOD

For the present study, 304 austenitic stainless-steel plates with dimensions of 100x100x6 mm were utilized. The chemical values of AISI 304 is shown in Table 1. The plasma welding schematic is illustrated in Figure 1. Argon was utilized as both the plasma and the shielding gas. The welding conditions for the samples are listed in Table 2.

Table 1. Chemical values of AISI 304 alloy.

Materials	Fe	Cr	C	Ni	Si	Mo	Mn
AISI 304	Bal.	19.2	0.042	8.25	0.46	0.25	1.75

Table 2. Welding conditions.

Sample no	S1	S2	S3
Current intensity (A)	70	80	90
Plazma gas flow speed (l/min)	0.5	0.5	0.5
Shielding gas flow speed (l/min.)	13	13	13
Travel speed (mm/min.)	0.01	0.01	0.01
Nozzle size (mm)	2.4	2.4	2.4

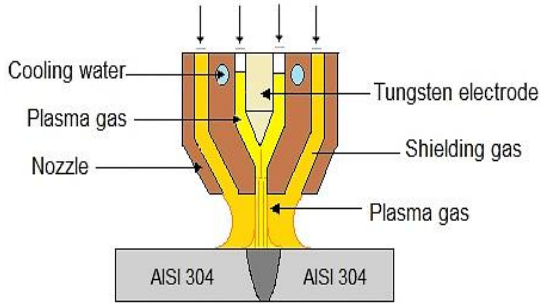

Figure 1. The plasma welding schematic.

The samples were welded in one pass using a Thermal Dynamics PS 3000 welding machine. Following the welding process, the samples were sanded with 220-1200 grit SiC sandpaper and subsequently polished with 3 µm diamond paste. The surfaces were electrolytically etched using 50% HNO_3 + 50% H_2O solution at 12 V for 10 s. The microstructure of the joint interface was analyzed using scanning electron microscopy (SEM: TESCAN MIRA3) and optical microscopy (OM: LEICA DM750). The chemical composition was identified through energy dispersive spectroscopy (EDS). The phases in the samples were identified using a Bruker D8 X-ray diffractometer. To detect the tensile strength of the joints, tensile samples were fabricated following ASTM E8 guidelines [13]. Dimensions of the tensile test samples are presented in Figure 2. These samples were tested on an Instron 8500 tensile machine at a tensile speed of 0.5 $mm{\cdot}min^{-1}$. The fracture surfaces of samples were studied by SEM.

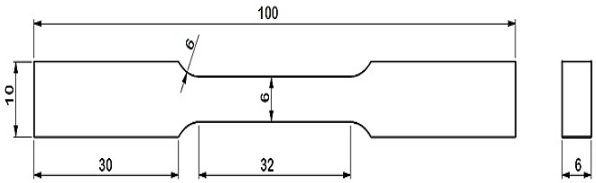

Figure 2. Dimensions of the tensile test samples.

3. RESULTS

3.1. Macro and microstructure

Macro visuals of the S1-S3 joints are presented in Figure 3. A smooth and clean surface in stainless steel joints was achieved using the PTA method. Heat input significantly influences the weld quality and visual appearance. Higher heat input results in the melting of a larger amount of material during the welding process [14]. The seam widths were measured as S1 = 6 mm at 70 A, S2 = 6.5 mm at 80 A, and S3= 7 mm at 90 A. A minimal extent was observed in both the HAZ and FZ. The PTA method achieved complete penetration in a 6 mm-thick 304 plate joint. The weld shape was thin and smooth. The level of heat input led to the development of a coarse microstructure. With increased heat input, the cooling rate diminished. The closed-loop current was directly related to the heat flux density. Consequently, raising the current intensity enhanced the heat input and temperature gradient, thereby enhancing thermo-capillary convection [15]. However, higher currents also intensified the electromagnetic and aerodynamic resistance forces. The electromagnetic force caused the weld pool to deepen. The aerodynamic friction force reduced the weld penetration and created a wider pool. At higher currents, the electromagnetic forces induced considerable mixing within weld material. This led to vortex formation that enhanced weld penetration and reduced bead width [16].

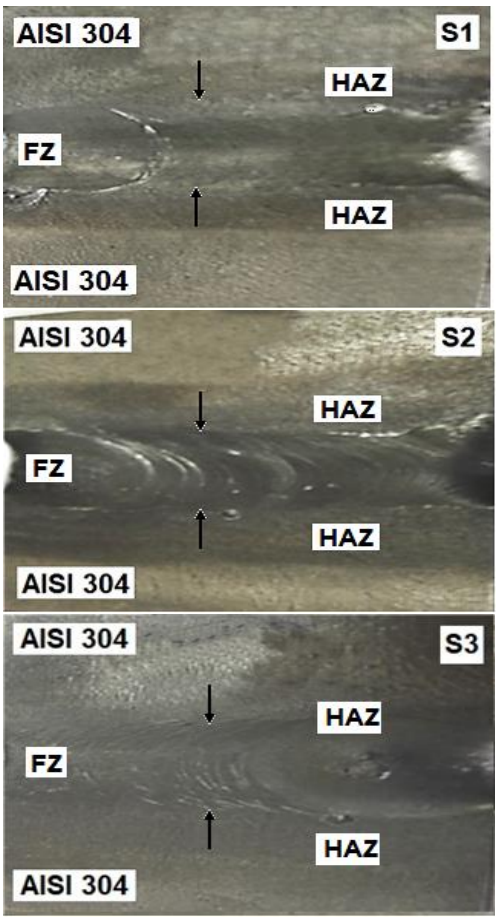

Figure 3. Macro view of S1-S3 joints.

Optical micrographs of the S1-S3 joints are presented in Figure 4. The welded zone, transition zone and HAZ are shown. At the interface, a columnar dendritic microstructure formed along the solidification direction as a result of the fast solidification of the stainless steel. SEM micrographs of S3 joint is given in Figure 5. Figure 5 exhibited the change of δ-ferrite morphology in the FZ. Lathy and skeletal δ-ferrite species were detected in the austenite matrix. With rising thermal input, the weld metal exhibited larger dendrites and wider interdendritic gaps. The alteration in dendrite shape resulted from sharp thermal gradients and rapid cooling caused by low heat input. This allowed less time for dendrite growth. Reduced cooling rates under high heat input provided adequate time for dendrite development in the fusion zone [17,18]. As heat intensity raised, the FZ and HAZ area also expanded. Significant grain growing is observed in the HAZ of all welds. Additionally, it was noted that the degree of grain growing incremented with higher heat intensity.

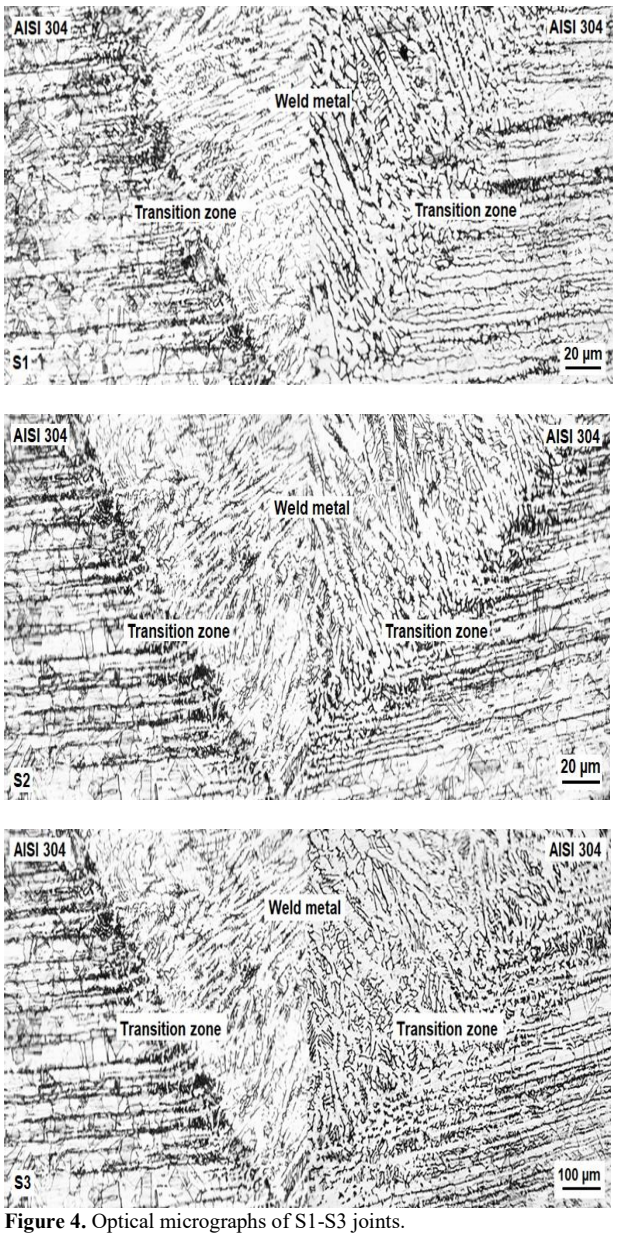

Figure 4. Optical micrographs of S1-S3 joints.

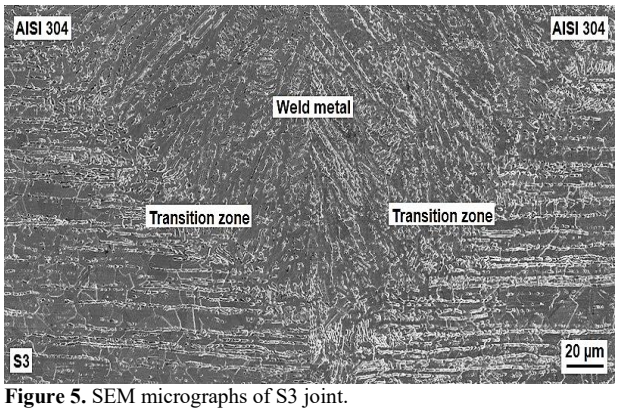

Figure 5. SEM micrographs of S3 joint.

EDS analysis points and results of S1 joint is shown in Figure 6. The presence of C, Fe, Cr, Ni, and Mn was verified by EDS. In the AISI 304 sample, the main elements that affected the phase compositions were Cr and Ni. Ni was depleted in the regions where Cr was enriched. In PTAW samples, the low thickness resulted in a high cooling rate and FA solidification mode. Solidification began with the formation of delta ferrite,

followed by peritectic-eutectic transformation and austenite nuclei. An intensified transformation took place with the increased cooling rate. This led to the formation of thinner austenite. The delta ferrite between the austenite layers also became thinner [19]. XRD graph of S3 joint is shown in Figure 7. The analysis revealed the presence of δ-Fe and γ-Fe.

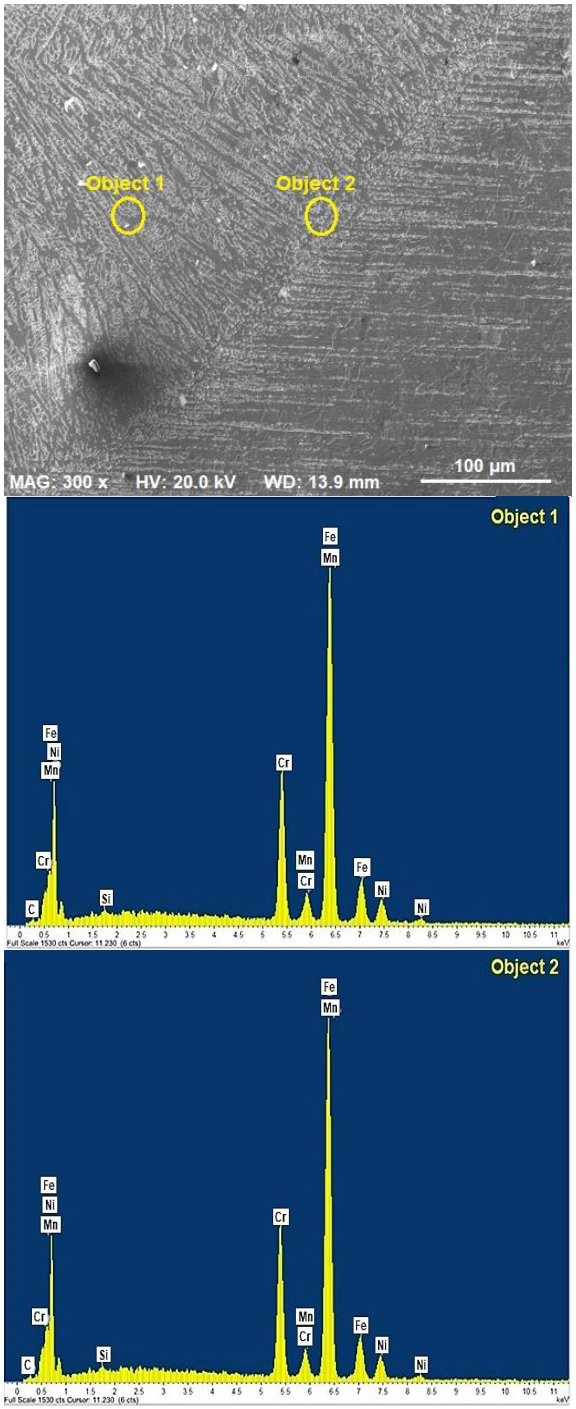

Figure 6. EDS analysis of S1 joint.

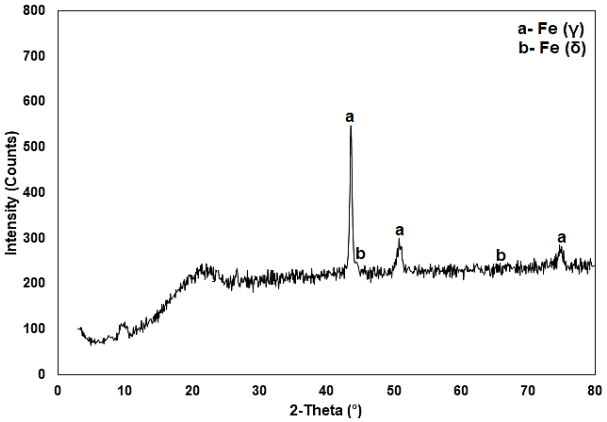

Figure 7. XRD graph of S3 joint.

3.2. Tensile behaviour

Macro images of samples are shown in Figure 8. The fracture of the welded 304 SS material took place in the HAZ. Stress-strain graph of samples is shown in Figure 9. The sample strength made with low heat intensity had 336 MPa, followed by 360 MPa for medium heat intensity, and 374 MPa for high heat intensity. Due to low current intensity, full penetration could not be achieved. This caused the disconnected sections at the interface to create a notch effect and weakened the strength. Increased welding current altered the intensity of forces during welding. Thus, affecting the flow of molten metal and the shape of the weld alloy. Higher heat input altered the weld metal microstructure and mechanical characteristics [19,20]. The weld strength was influenced by the HAZ of the weld alloy. In PTAW, the volume of melt alloy was comparatively low at any moment, resulting in quicker cooling of the weld metal and a smaller weld zone size [21]. During PTAW, fluid movement in the molten area intensified, leading to a reduction in grain size within the weld metal. The increased heat input advanced the occur of more δ-ferrite in PTAW. Ferrite formation may take place at low temperatures with restricted diffusion due to the enrichment of ferrite stabilizers like Cr and the depletion of austenite stabilizers such as Ni. During rapid solidification, δ-ferrite can stay in a metastable state, failing to fully transform into the γ phase. The Cr-enriched interdendritic δ-ferrite in the microstructure can significantly hinder the dislocation motion [2,21]. The advanced δ-ferrite structure alleviates localized stress in surrounding phases, promoting a more uniform austenite transformation. As a result, the retained austenite exhibits enhanced mechanical stability and improved ductility [23]. The δ-ferrite in the weld material minimized microcracks, refined the particle shape, improved ductility, and helped prevent susceptibility to hot cracking in the weld.

Figure 8. Macro image of samples.

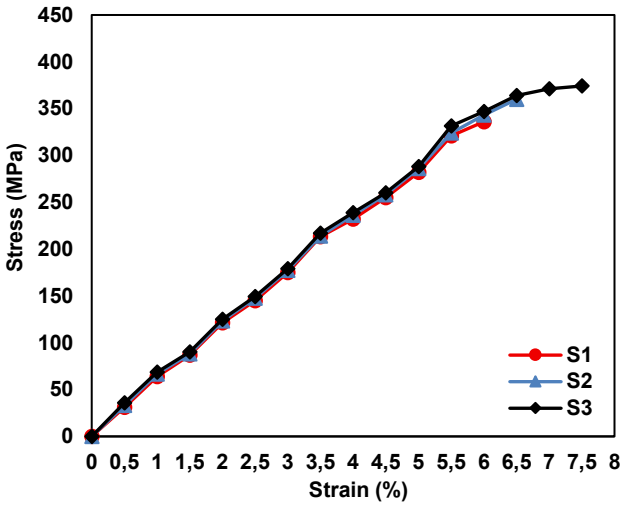

Figure 9. Stress-strain graph of samples.

3.4. Fracture characteristics

Figure 10 displays the fracture characteristics of the S1 joint. The fracture surfaces exhibited dimples of different sizes and shapes, suggesting that the primary fracture mechanism was ductile in nature [24]. With the increase in crack growth rate near the fracture zone, the merging of voids along with pits and lines became evident. Distinct pit formations were present in the rapid fracture area. Voids originating from inclusions or larger precipitates expanded and developed a fibrous texture as yielding progressed [25-27].

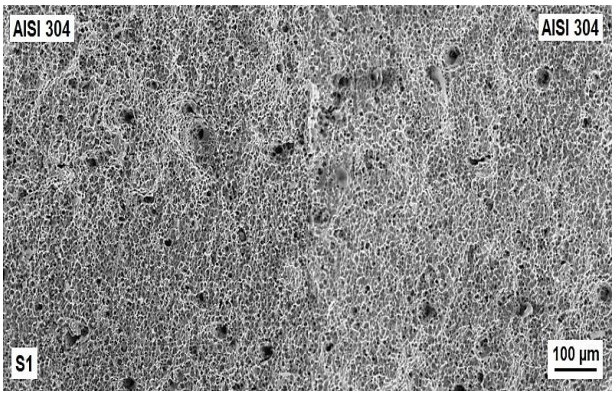

Figure 10. Fracture characteristics of S1 joint.

4. CONCLUSION

AISI 304 plates were joined using the PTAW. The following insights can be gathered from this study.

1. The 304 stainless plates with full penetration were obtained by using PTAW.
2. A smooth and clean surface in stainless steel joints was achieved using the PTAW.
3. The samples exhibited strengths of 336 MPa at 70 A, 360 MPa at 80 A, and 374 MPa at 90A.
4. For 6 mm thick AISI 304, the PTA process offered a wide range of parameters.
5. Ductile pits of different sizes and shapes were detected on the fracture surfaces.

Acknowledgement

The authors declare no conflict of interest.

REFERENCES

[1] Yan J, Gao M, Zeng X. Study on microstructure and mechanical properties of 304 stainless steel joints by TIG, laser and laser-TIG hybrid weldings. Opt Lasers Eng. 201048(4):512-7.

[2] Lippold JC, Kotecki DJ. Welding metallurgy and weldability of stainless steel. 5nd ed. New York, USA: John Willey & Sons; 2005.

[3] Zumelzu E, Sepulveda J, Ibarra M. Influence of microstructure on the mechanical behaviour of welded 316 L SS joints. J Mater Process Technol. 1999;94(1):36-40.

[4] Korinko PS, Malene SH. Considerations for the weldability of types 304L and 316L stainless steel. Pract Fail Anal. 2001;1:61-8.

[5] Shyu SW, Huang HY, Tseng KH, Chou CP. Study of the performance of stainless steel A-TIG welds. J Mater Eng Perform. 2008;17:193-201.

[6] Kumar S, Shahi AS. Effect of heat input on the microstructure and mechanical properties of gas tungsten arc welded AISI 304 stainless steel joints. Mater Des. 2011;32(6):3617-23.

[7] Mirshekari GR, Tavakoli E, Atapour M, Sadeghian B. Microstructure and corrosion behavior of multipass gas tungsten arc welded 304L stainless steel. Mater Des. 2014;55:905-11.

[8] Teker T. Effect of melt-in and key-hole modes on the structure and mechanical properties of AISI 430 steel welded using plasma transfer arc welding. Phys Metals Metallogr. 2018;119(7): 669-77.

[9] Singh NK. Performance of activated TIG welding in 304 austenitic stainless steel welds. Mater Today. 2017;4(9):9914-18.

[10] Ogundimu EO, Akinlabi ET, Erinosho MF. Study on microstructure and mechanical properties of 304 stainless steel joints by TIG–MIG hybrid welding. Surf Rev Lett. 2018;25(01):1850042.

[11] Bodkhe SC, Dolas DR. Optimization of activated tungsten inert gas welding of 304L austenitic stainless steel. Procedia Manuf. 2018;20:277-82.

[12] Ramakrishnan A, Rameshkumar T, Rajamurugan G, Sundarraju G, Selvamuthukumaran D. Experimental investigation on mechanical properties of TIG welded dissimilar AISI 304 and AISI 316 stainless

steel using 308 filler rod. Mater Today. 2021;45(9):8207-11.
[13] ASTM E8M-04, Standard test methods for tension testing of metallic materials. West Conshohocken, PA, USA, ASTM International; 2004.
[14] Taufiqurrahman I, Ahmad A, Mustapha M, Ginta TL, Haryoko LAF, Shozib, IA. The effect of welding current and electrode force on the heat input, weld diameter, and physical and mechanical properties of SS316l/Ti6Al4V dissimilar resistance spot welding with aluminum interlayer. Mater. 2021;14(5):1129.
[15] Somani CA, Lalwani DI. Experimental investigation of TIG-MIG hybrid welding process on austenitic stainless steel. Mater Today. 2019;18(7):4826-34.
[16] Prasad KS, Rao CS, Rao DN. Study on weld quality characteristics of micro plasma arc welded austenitic stainless steels. Procedia Eng. 2014;97:752-57.
[17] Zhang L, Lu ZJ, Luo KY, Feng AX, Dai FZ, Zhong JS, Luo M, Zhang YK. Residual stress, micro-hardness and tensile properties of ANSI 304 stainless steel thick sheet by fiber laser weldings. Mater Sci Eng: A. 2013;56:136-44.
[18] Cui S, Liu Z, Fang Y, Luo Z, Manladan S M, Yi S. Keyhole process in K-TIG welding on 4 mm thick 304 stainless steel. J Mater Process Technol. 2017:243;217-28.
[19] Feng Y, Luo Z, Liu Z, Li Y, Luo Y, Huang Y. Keyhole gas tungsten arc welding of AISI 316L stainless steel. Mater Des. 2015;85:24-31.
[20] Lee WS, Lin CF. Impact properties and microstructure evolution of 304L stainless steel. Mater Sci Eng: A. 2001;308(1-2):124-35.
[21] Saha S, Mukherjee M, Pal TK. Microstructure, texture, and mechanical property analysis of gas metal arc welded AISI 304 austenitic stainless steel. J Mater Eng Perform. 2015;24:1125-39.
[22] Ramkumar KD, Singh S, George JC, Anirudh S, Brahadees G, Goyal S, Gupta SK, Vishnu C, Sharan NR, Kalainathan S. Effect of pulse density and the number of shots on hardness and tensile strength of laser shock peened, activated flux TIG welds of AISI 347. J Manuf Proces. 2017;28(1):295-308.
[23] Liu M, Li Y, Cui Z, Yang Q. High ductility of spray formed low density TRIP steel with the improvement of δ-ferrite matrix. Mater Charact. 2019;156:109828.
[24] Abioye TE, Gbadeyan OO, Adebiyi DI. Analysis of the mechanical properties and penetration depth of gas metal arc welding on AISI 304 stainless steel. Int J Microstruct Mater Prop. 2019;14(1):47-9.
[25] Puchi-Cabrera ES, Saya-Gamboa RA, La Barbera-Sosa JG, Staia MH. Ignoto-Cardinale V, Berríos-Ortiz JA, Mesmacque G. Fatigue life of AISI 316L stainless steel welded joints, obtained by GMAW. Weld Int. 2009;23(10):778-88.
[26] Sabzi M, Dezfuli SM. Post weld heat treatment of hypereutectoid hadfield steel: characterization and control of microstructure, phase equilibrium, mechanical properties and fracture mode of welding joint. J Manuf Process. 2018;34:313-28.
[27] Haldar V, Biswal SK, Pal S. Formability study of micro-plasma arc-welded AISI 316L stainless steel thin sheet joint. J Braz. Soc Mech Sci Eng. 2022;44:564.